IET Microwaves, Antennas & Propagation

Research Article

IET Journals
The Institution of Engineering and Technology

Broad-band embroidered spiral antenna for off-body communications

ISSN 1751-8725
Received on 31st December 2015
Revised on 25th May 2016
Accepted on 21st July 2016
doi: 10.1049/iet-map.2015.0848
www.ietdl.org

Shiyu Zhang[1] ✉, Anastasios Paraskevopoulos[1], Cyril Luxey[2], Jon Pinto[3], William Whittow[1]

[1]*The Wolfson School of Mechanical, Electrical and Manufacturing Engineering, Loughborough University, Leicestershire, UK*
[2]*EpOC, University Nice-Sophia Antipolis, Valbonne, France*
[3]*BAE Systems, Applied Intelligence Labs, Advanced Technology Centre, Gt. Baddow, Chelmsford, UK*
✉ *E-mail: S.Zhang@lboro.ac.uk*

Abstract: An embroidered wearable spiral antenna is presented in this study. The spiral antenna is compact and flexible, yet has broad-band performance. The novelty of this study includes considering the antenna–body interaction rather than just considering the antenna alone. The antenna has been simulated and measured on a specific anthropomorphic mannequin torso phantom and a real person. The far-field on-body performance of the embroidered antenna on the phantom has been measured using a novel cylindrical near-field to far-field transformation technique. This technique allows the fast extraction of the full spherical radiation pattern and the corresponding far-field antenna characteristics on the human body without the need of rotating the phantom with expensive positioning systems. The on-body antenna performance including realised gain, directivity, radiation efficiency, radiation pattern and axial ratio have been presented.

1 Introduction

Wearable technology has been implemented into our daily lives and is becoming a rapidly growing market in recent years. The modern wearable devices are required to be light-weight, low-profile, but also multifunctional and wirelessly connected, which means they can be applied in location tracking, health monitoring and on-body networks. A smart-cloth which is made by using specialised fibres integrating multifunctional electronics into everyday clothing is an ideal candidate for wearable devices [1, 2]. Furthermore, one of the key advantages of flexible wearable antennas at frequencies of the order of 400 MHz–1 GHz is that the antenna can be the size of the torso without compromising the comfort to the user when the antennas are integrated into clothing. Therefore, the antenna performance is not compromised by the need for size reduction.

One challenge of designing antennas for wearable devices is overcoming the dielectric loading and de-tuning due to the presence of human body [3]. The antenna performance such as gain, radiation efficiency and radiation pattern are also strongly affected by the body shape which results in the antenna being sensitive to its position on the human body. Therefore, it is important to include the human body as part of the wearable antenna design.

There are many potential applications for wearable antennas that include medical monitoring and hypothermia [4], radiofrequency identification tags, medical sensors [5], communication bands between 400 MHz and 3 GHz which include ultra-high frequency (UHF), medical implant communications service (MICS), industrial, scientific and medical (ISM), ultra-wideband [6] and also energy harvesting. The broad-band antennas demonstrated here do have a number of applications in the sportswear/recreation, emergency services, security and defence areas as part of an 'off-body' network. Typical examples might be where fire-fighters are required to enter areas of poor visibility in buildings or where search and rescue teams need to operate in bad weather such as blizzards, fog or smoke. The broad-band nature of the devices lend themselves to high data-rate communications with fault tolerant modulation schemes such as orthogonal frequency division multiplexing or direct-sequence spread spectrum with significant forward error correction.

The 300 MHz–3 GHz full UHF band coverage of the spiral provides opportunities for supporting transmission and reception at high data rates such as those associated with high definition video from body worn cameras. Such a wideband system might thus carry, voice, visual and perhaps thermal infra-red video, in addition to co-ordinates derived from global positioning system (GPS) or inertial based sensors. The wideband nature of the antenna also makes it well suited for use with future software defined radio equipment. The UHF band is particularly densely packed with communications channels because it is sufficiently high in frequency to support useful data-rates, but sufficiently low that transmission of the signal through walls and other obstacles/or around them by diffraction, is also a significant effect. Some of these existing UHF communications channels, particularly digital ones, can be exploited for novel techniques such as body worn NAVigation using Signals of Opportunity. This allows a wide range of signals of different frequencies and polarisations to be used as the basis for navigation in GPS denied environments. UHF coverage includes the Global System for Mobile (GSM) bands, digital video broadcasting (DVB) and digital audio broadcasting (DAB) frequency broadcasts, which are all suitable for this purpose.

Therefore, a wideband antenna offers the flexibility to function at various frequencies. This paper reports on an antenna that has not been designed for a specific frequency, but rather the interaction of the antenna with the human body has been investigated over a range of frequencies.

The fabrication techniques of wearable antennas have been reviewed in [7]. Embroidery is a promising technique. Conductive fabrics are textile-based materials which have the features of ordinary textiles such as flexibility and integration into fabrics in the manufacturing process. To date, a wide range of research has been carried out to investigate the performance of the conducting fabric for high-frequency applications including antennas and frequency selective surfaces [8].

The flexible fabric antennas can be concealed inside the inner lining of clothing [9]. The textile-based wearable devices are expected to be suitable for mass-manufacture, which would substantially reduce the manufacturing cost. The stitch spacing, direction and density affect the performance of embroidered antennas. The stitch direction should be aligned along the main current flow direction and high stitch densities improve electrical performance at the expense of loss in flexibility [10]. The electromagnetic performance of conducting textiles at gigahertz frequencies has been outlined in [11, 12]. Embroidery is an excellent choice of manufacturing technique for spiral antennas as

it is challenging and wasteful to cut the delicate shapes out of a continuous metal textile cloth.

Spiral antennas are a popular type of antenna due to their large bandwidth and low profile. Various papers have considered wearable spiral antennas [4–6, 13–15]. Various embroidered spiral antennas have been considered in the last couple of years [5, 6, 14, 15]. The density of the embroidered threads has been increased where the currents were largest [6]. Different fabrication techniques have been compared in [2]. Spiral antennas have been placed on metallic cylinders [14, 15] and on a small cuboid sponge material [4]. None of these papers considered the effect of the body which is critically important to the behaviour of the antenna. Therefore, though similar designs have been previously reported, the effect of the body on the spiral antenna is novel.

Gain and efficiency measurements of antennas on the human body are very difficult. Owing to the large size and weight of the specific anthropomorphic mannequin (SAM) phantom there is an inherent difficulty in measuring the wearable spiral antenna with the conventional far-field measurement technique. For this reason, the far-field results in this paper were obtained by using a novel cylindrical near-field measurement methodology. The near-field results were then transformed to the far-field domain. Far-field parameters such as gain, directivity and efficiency have been produced for the spiral antenna placed directly against the phantom's surface. In addition, the effect of the human body on the circular polarisation of the spiral antenna has been determined through the information of the axial ratio (AR) that is calculated from the measurement results.

This paper has investigated the performance of an embroidered spiral antenna on an SAM torso phantom and also on a real human. Section 2 presents the simulation of the spiral antenna on the SAM torso phantom using computer simulation technology (CST) Microwave Studio (CST). The authors have previously simulated a planar spiral design simulated on a cuboid phantom [16]. However, since the embroidered antenna is flexible which can be tightly fitted on the body to adjust the body shape, more complex simulations were carried out on the effects of bending the spiral antenna and the effects of the distance between the antenna and body. The fabrication of the embroidered spiral antenna is presented in Section 3. The antenna design is exported as a graphical format to the digital embroidery machine and fabricated at the Loughborough University. Section 4 includes an impedance transformer to improve the match. This section also includes $|S_{11}|$ measurement of the embroidered antenna on a real human. The far-field performance including realised gain, directivity, radiation efficiency, radiation pattern and AR of the spiral antenna on the SAM torso phantom have been measured using near-field to far-field transformations method and presented in Section 5. The final conclusions are made in Section 6.

2 Spiral antenna design

The Archimedean spiral antenna was designed to operate over a wideband frequency range from 300 MHz to 3 GHz. The width of each line was 5.8 mm; the spacing between lines was 6.0 mm and the exterior diameter of the whole spiral was 208 mm. In the simulation, the two arms of the spiral were modelled as 1 μm thick and with the conductivity of silver, which emulated the conductive thread Liberator™. The spiral antenna was placed on the abdomen of the SAM torso phantom. The physical SAM phantom was manufactured by MCL-T [17] with geometrical characteristics according to the IEC62209-2 Standard. The phantom is made of carbon-loaded silicone rubber with dielectric properties to match human body tissue over the 0.03–6 GHz frequency range. The dielectric properties of the phantom material followed the MCL-T broad-band tissue-equivalent recipe which was based on 2/3 muscle tissue properties. The dielectric properties of the SAM phantom at selected frequencies are shown in Table 1. Note, in the simulations, the clothing between the spiral antenna and body was not included. The design for the antenna in CST can be seen in Fig. 1.

Table 1 Dielectric properties of the SAM phantom

Frequency, GHz	Relative permittivity	Conductivity, S/m
0.48	50.1	0.6
0.97	42.6	0.9
1.46	39.0	1.2
1.97	36.8	1.6
2.41	35.4	1.8
2.95	33.9	2.1

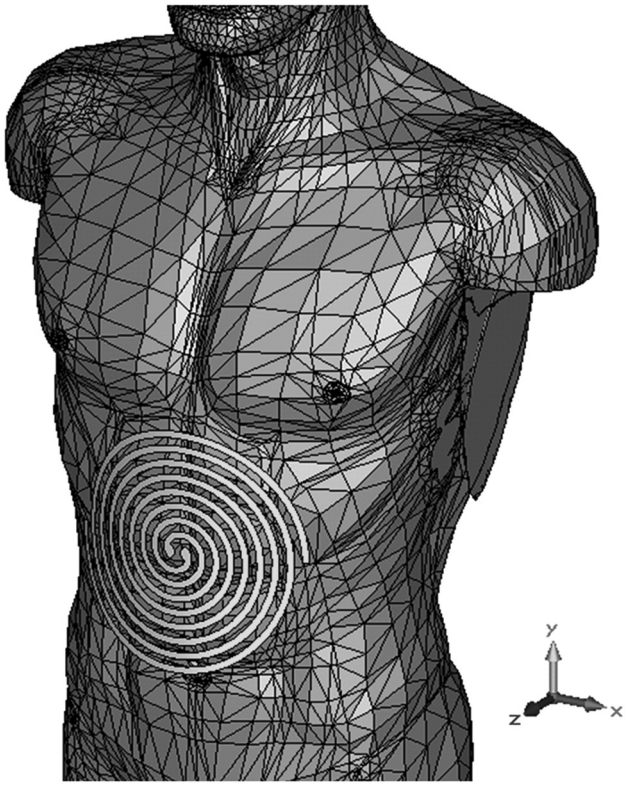

Fig. 1 *Curved spiral antenna on the SAM phantom simulation in CST*

The simulated $|S_{11}|$ of the antenna on the phantom over the frequency ranging from 0.3 to 3 GHz for four different spacing (2, 7, 12 and 17 mm) between antenna and body are shown in Fig. 2*a*. The 2 mm distance was approximately equal to a thin T-shirt between the antenna and a human body. All the separations have $|S_{11}|$ generally lower than −5 dB for almost the whole frequency range above 0.5 GHz. Fig. 2*b* shows the simulated $|S_{11}|$ of the curved antenna, compared with the planar antenna. The antenna is curved on *Y*-axis with 30°, 40° and 50° curvature angles. The centres of the antennas with different curved angles remained at 2 mm distance from the phantom. Larger curving angles result in the ends of the two spiral arms closer to the phantom which emulates that the antenna is more tightly fitted on the body. The simulated results indicate that the $|S_{11}|$ were deteriorated by 0.5–1 dB at the frequency ranges of 0.8–1.0 GHz and 1.4–2.0 GHz, but no significant impact on other frequency ranges. In addition, the $|S_{11}|$ differences between the different curvature angles are negligible. However, the weak impedance matching is due to the larger impedance of the spiral while the input impedance is 50 Ω. The simulations indicated that the optimal input impedance was ∼150 Ω. Therefore, a 3:1 impedance transformer can be used to improve the S_{11} results. Simulation indicates that the radiation efficiency of the spiral antenna is not affected by the transformer. The measurement results of the embroidered spiral antenna with the impedance transformer between the feed cable and the antenna are presented in Section 4.

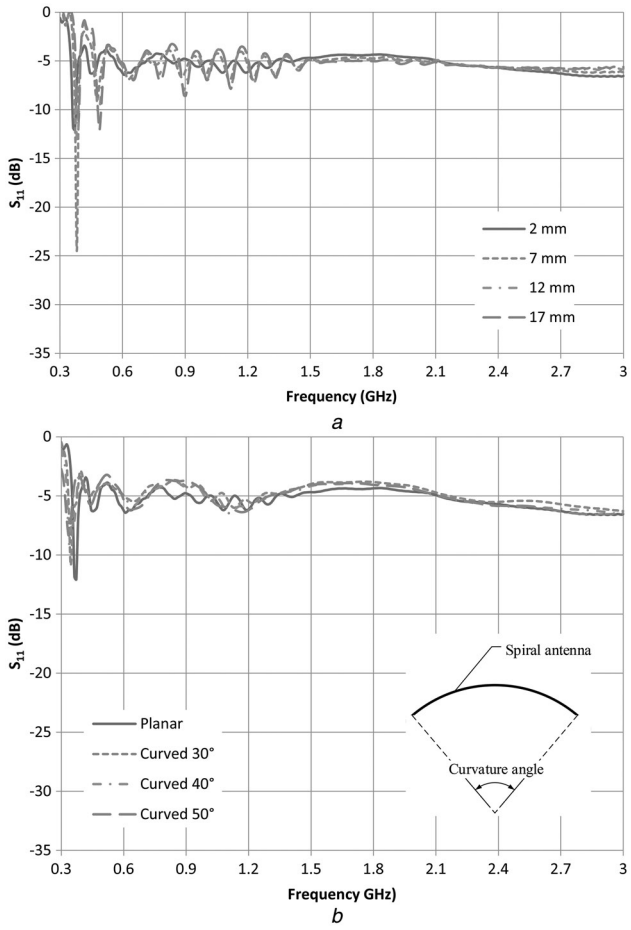

Fig. 2 *Simulated $|S_{11}|$ of the spiral antenna on the SAM phantom*

a Planar spiral antenna of different distances from SAM phantom
b Different curvatures of the spiral antenna on the SAM phantom

The simulated far-field simulation at 2.4 GHz of the 50° curved spiral antenna on phantom is shown in Fig. 3. This figure clearly shows that the back side of the radiation pattern (90°–270°) was distorted by the phantom which is located behind the antenna and the whole pattern becomes more directional. The spiral antenna is expected to be circular polarised and Fig. 3 shows that the level of E-θ and E-ϕ components are very similar at the boresight (0°). AR level is used to examine the circular polarisation performance of the spiral antenna. The simulated AR at the boresight of the spiral antenna on phantom with 50° curvature at 2.4 GHz is 1.22 dB, which shows the simulated antenna is circular polarised even when it was curved and placed close to the phantom. A simulation of the specific absorption rate (SAR) also has been carried out to investigate the level of the radiated power that is absorbed by the body. The simulated SAR level is 15.7 W/kg averaged over 10 g with a 1 W input power at 2.4 GHz. Therefore, the input power should be limited to below 0.13 W to comply with the International Commission on Non-Ionizing Radiation Protection SAR standards which is 2 W/kg [18]. Note, for military personnel, SAR values five times higher than for the general population are allowed. The simulated SAR over 10 g with 0.13 W input power at 2.4 GHz is shown in Fig. 4.

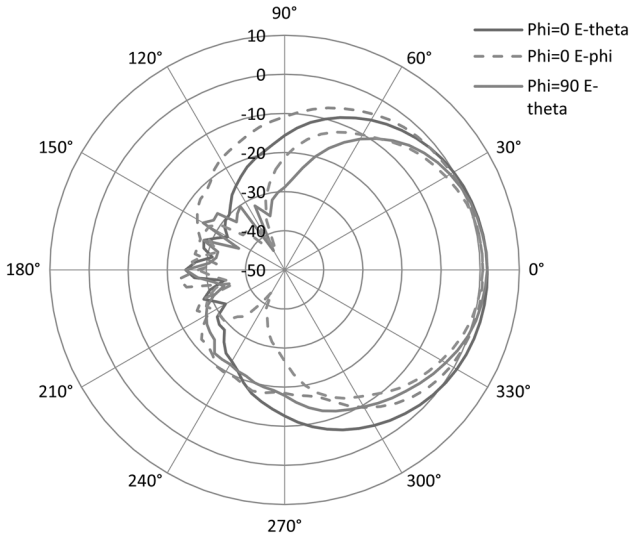

Fig. 3 *Simulated gain pattern of the 50° curved spiral antenna 2 mm from SAM phantom at 2.4 GHz ($\phi = 0°$ is the XOZ-plane whilst $\phi = 90°$ is YOZ-plane)*

The simulated radiation efficiencies of the spiral antenna on the SAM phantom are shown in Fig. 5. This shows a logical trend that with the increased distance in terms of wavelengths between the antenna and body, the efficiency of the antenna is increased. On the other hand, increased curvature decreases the antenna efficiency, but not significantly (~2% reduction). Since all the curved antennas have the same 2 mm distance from the centre to the phantom, it can be concluded that the distance between the antenna and human body is more important compared with the curved angle of the spiral antenna. The efficiencies of different curved angles are very similar, which indicates that this spiral antenna can be tightly fitted on the body and curving does not significantly affect its performance.

3 Fabrication of embroidered spiral antenna

The spiral antenna was embroidered by using the Entrepreneur Pro PR1000e digital embroidery machine. Silver-coated conducting thread Liberator™ [19] has been used for embroidery. The base cloth was cotton and was 0.5 mm thick. The stitch direction of the embroidered threads followed the current flow direction for giving the optimal performance. Higher number of stitches, shorter stitch length and closer stitch spacings improved the density and robustness of the embroidered pattern, at the cost of losing flexibility. However, for a medium-density embroidery setting, it still required more than 12,000 individual stitches which represented more than 120 m of thread, to complete the spiral pattern. This made it time consuming and costly to fabricate this spiral antenna. To reduce the expense of fabrication, 4 cm stitch length was used and each single arm of the spiral was formed by four parallel stitches. The final antenna consisted of ~4500 individual stitches with an approximate length of 45 m of Liberator thread. Meanwhile, the thread tension was also carefully adjusted to ensure it was suitable for the antenna design using the specialised threads. Tension that was too tight caused warping of the base fabric also the embroidered pattern, and even breaking of the thread. On the other hand, tension that was too loose resulted in a poorly defined embroidered pattern. The embroidered spiral antenna is shown in Fig. 6. The embroidered spiral antenna was fed by a 50 Ω flexible coaxial cable. A low-temperature solder was used to avoid damaging the base fabric (white fabric in Fig. 6). The other end of the cable was connected to a vector network analyser (VNA) for testing.

4 Adding an impedance transformer and on-body antenna measurements

The previous simulations showed the impedance could be improved by using a 150 Ω feed impedance. A 3:1 impedance transformer was used to transfer the 50 Ω input impedance to 150 Ω in order to match the impedance of the spiral antenna. The transformer was soldered to the two arms of the spiral. The embroidered spiral antenna was

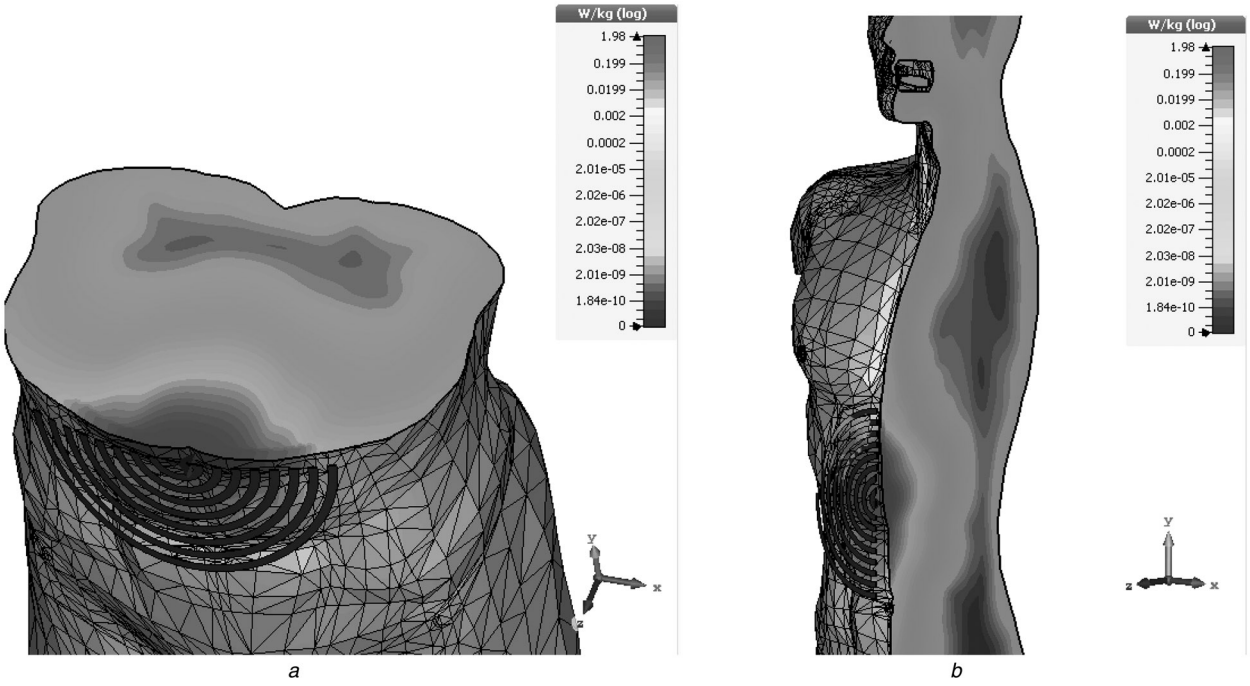

Fig. 4 *Simulated SAR of the 50° curved spiral antenna 2 mm from SAM phantom at 2.4 GHz*

a XOZ cut plane view
b *YOZ* cut plane view

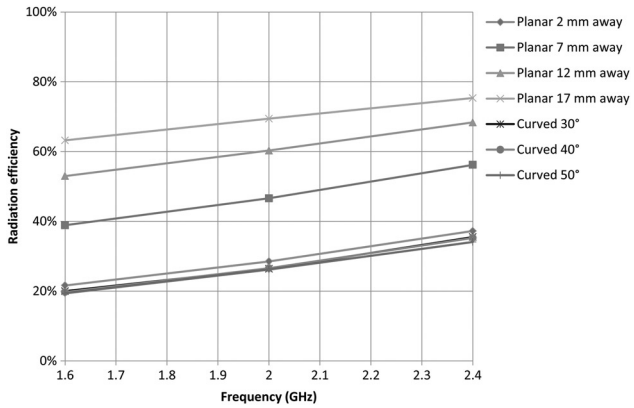

Fig. 5 *Simulated radiation efficiencies of the spiral antennas on SAM phantom*

measured when placed against a real person wearing a jumper. The measured $|S_{11}|$ result is shown in Fig. 7. The simulated and measured S_{11} results of the planar antenna with the transformer in free space are included for comparison. The antenna against the human abdomen has an $|S_{11}|$ below −8 dB between 0.9 and 3 GHz. It can be clearly seen in Fig. 6 that the substrate and antenna have been slightly warped due to the tension of the embroidered threads. The inherent flexibility of wearable antennas inevitably means that there will be discrepancies between simulations and measurements.

5 Antenna measurements on SAM phantom

The fabricated embroidered spiral antenna was measured on the SAM phantom using the cylindrical near-field measurement technique. The cylindrical near-field measurement system inside the anechoic chamber included a linear scanning axis positioner and an azimuth turntable, see Fig. 8. The axis system was fixed with the *Z*-axis facing the probe's aperture.

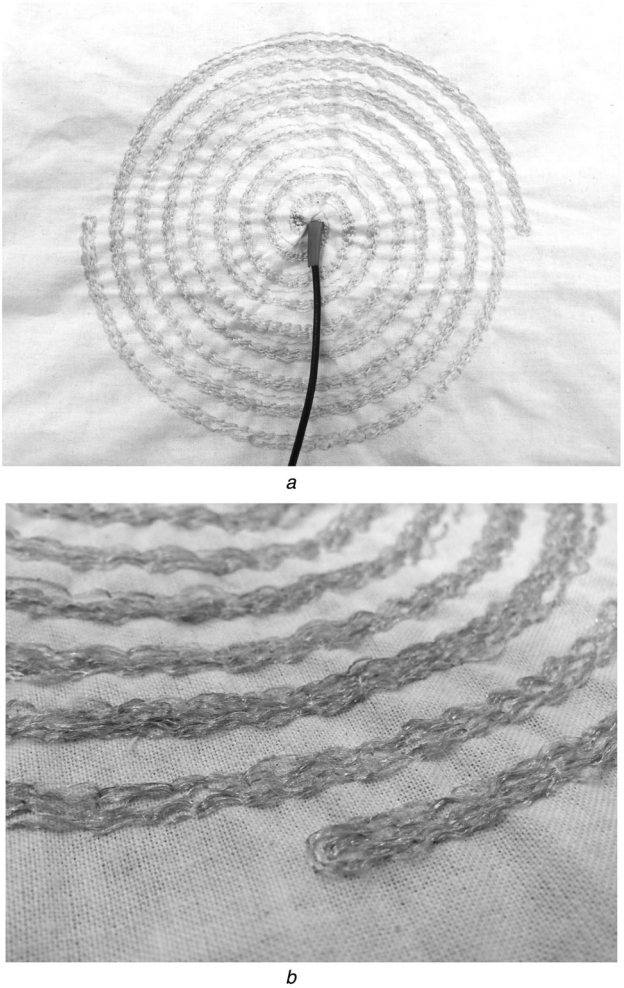

Fig. 6 *Embroidered spiral antenna*

a Top view
b Zoomed in view

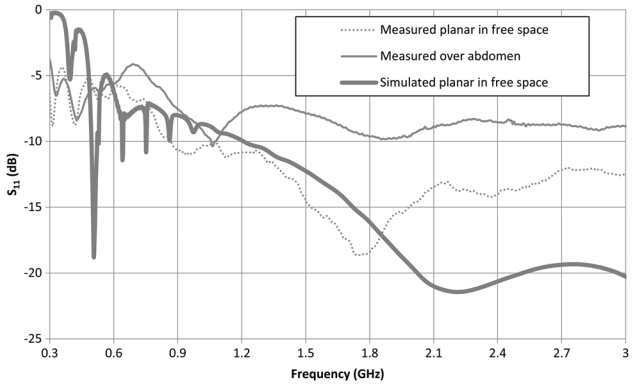

Fig. 7 *Measured $|S_{11}|$ of embroidered spiral antenna in free space and when placed over human abdomen*

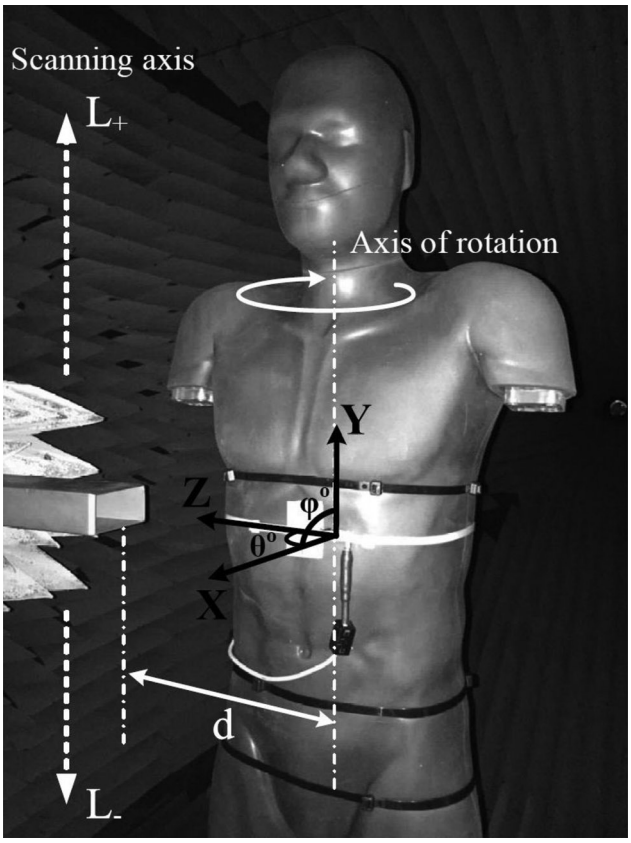

Fig. 8 *SAM phantom, near-field probe and scanning geometry*

An open-ended rectangular waveguide probe operating at 1.6–2.6 GHz (WR-430) scanned along the *Y*-axis and was connected at the Tx port of a VNA. The embroidered spiral antenna, which was placed on the surface of the SAM phantom, was rotated in azimuth using the turntable while being connected at the Rx port of the VNA. By rotating the waveguide probe by 90°, two orthogonal *E*-field components were measured (in amplitude and phase) in the near-field range of the antenna under test (AUT). The recorded near-field data are gathered in a cylindrical surface close to SAM body surface ($d = 3\lambda$). This close distance in the *Z*-axis was selected in conjunction to the finite scanning length ($L = 3.5$ m) in the *Y*-axis in order to minimise the scan area truncation error that becomes evident in the far-field patterns at elevation angles around 90°, after the near-field to far-field transformation [20].

The spiral was positioned on the abdomen of the SAM torso phantom, see Fig. 9. This phantom does not have an insulating

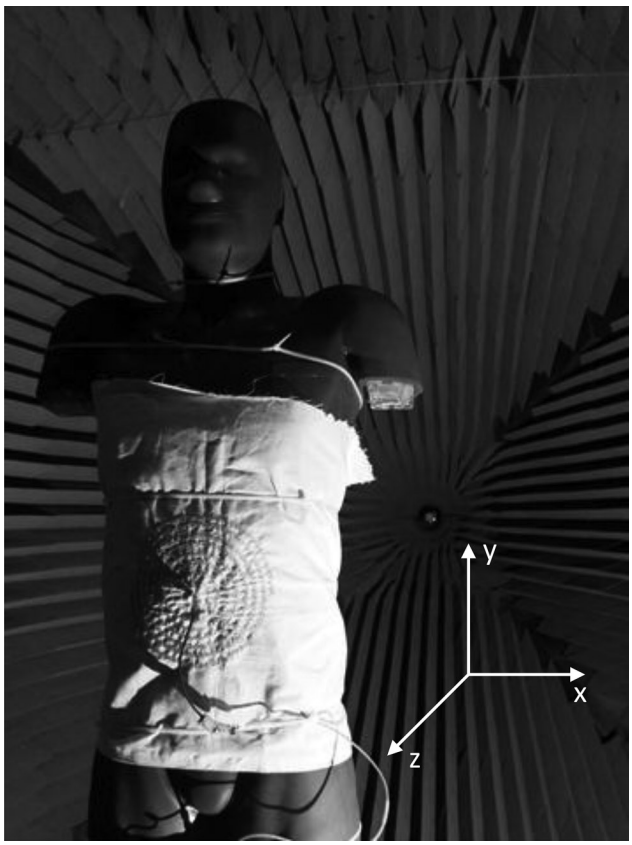

Fig. 9 *Embroidered spiral antenna attached to the SAM torso phantom in tapered anechoic chamber*

plastic shell. The permittivity and conductivity of the phantom at selected frequencies are given in Table 1. Note the phantom consisted of the torso only, without arms or legs.

The measured $|S_{11}|$ of the spiral antenna on the SAM phantom indicates that the SAM phantom is a very good approximation to the real human body over the frequency range considered [16].

The computed far-field characteristics from 1.6 to 2.6 GHz are shown in Table 2. The radiated gain is the value in the maximum direction of radiation. As can be seen from Fig. 9, the antenna has been placed flush against the torso. Therefore, the antenna has been measured in the worst-case scenario. Therefore, sections of the conducting thread are <2 mm away from the lossy torso. As a comparison, a perfect electrically conducting dipole operating at 2 GHz and placed 3 mm from a cuboid body phantom had a simulated radiation efficiency of 8%. Note the radiated gain and the radiation efficiency do not include the $|S_{11}|$ mismatch. The antenna radiated gain increased from 0.29 dBi at 1.6 GHz to 3.4 dBi at 2.6 GHz. At higher frequencies, the antenna–phantom separation in wavelengths increased which resulted in the enhanced efficiency. Additionally at higher frequencies, the skin depth decreases, and therefore the thickness of the metallisation of the conducting thread (in terms of skin depths) increases which means the thin (~1 μm)

Table 2 Computed far-field characteristics from near-field measurements of the embroidered spiral antenna on the phantom. (*© 2015 IEEE* [16])

Frequency, GHz	Directivity, dBi	Radiated gain, dBi	Radiation efficiency, %
1.6	9.36	0.29	12.4
1.8	9.45	1.69	16.8
2.0	9.57	2.69	20.5
2.2	10.14	3.12	19.9
2.4	9.98	3.00	20.0
2.6	10.12	3.40	21.3

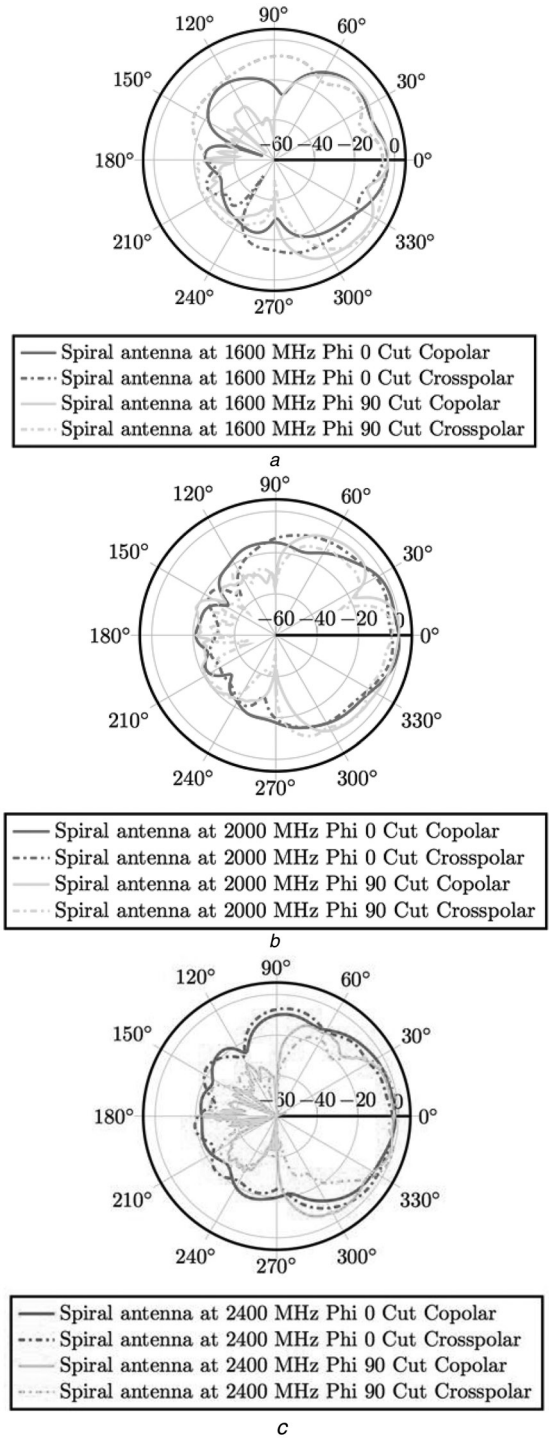

Fig. 10 *Computed radiated gain patterns of the embroidered spiral antenna on SAM phantom ($\phi = 0°$ is the XOZ-plane whilst $\phi = 90°$ is the YOZ-plane). ϕ 0 cut copolar → G_φ (vertical field component); ϕ 0 cut cross-polar → G_θ (horizontal field component); ϕ 90 cut copolar → G_φ (vertical field component); ϕ 90 cut cross-polar → G_θ (horizontal field component) (© 2015 IEEE [16])*

a At 1600 MHz
b At 2000 MHz
c At 2400 MHz

conducting thread can better support the currents which leads to higher efficiencies.

The radiation patterns at 1.6, 2.0 and 2.4 GHz of the embroidered spiral antenna on the SAM phantom are shown in Fig. 10. The radiation patterns at all the frequencies are distorted between 90° and 270°, which is due to the interaction (power absorption) with

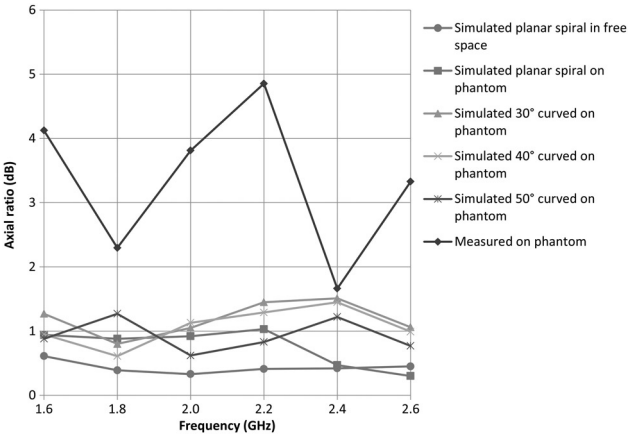

Fig. 11 *Measured AR of spiral antenna on SAM phantom compared with simulations*

the torso phantom. This effect is in good agreement with the simulation. The radiation pattern becomes more directional at $\theta = 0°$ with the increased frequency. The unavoidable truncation error is also evident in the $\phi = 90°$ patterns, for angles around $\theta = 90°$.

The measured and simulated results of the AR level at the boresight ($\theta = 0°$) from 1.6 to 2.6 GHz of the spiral antenna on the phantom are shown in Fig. 11. The simulation results of the planar spiral antenna in free space and on the phantom indicate that the AR of the antenna is increased by ∼0.5 dB up to 2.2 GHz due to the phantom behind. Furthermore, the curving of the spiral antenna does not significantly affect the AR level and all the simulated AR are generally smaller than 1.5 dB from 1.6 to 2.6 GHz at boresight, which shows all the curved spirals have good wideband circular polarisation performance when placed on the phantom. However, the measured AR were generally higher than the simulated values, but still have the AR < 3 dB at 1.8 and 2.4 GHz. These results are comparable with previous papers who achieved ARs of up to 5 dB (and above at some frequencies) when the embroidered antenna with a ground plane was placed on a metal cylinder [14]. The absence of a ground plane in this paper and the variables created by using a realistic phantom means these results are reasonable. The difference between simulated AR and measurement is due to imperfections of the embroidered pattern. As the tension of the threads made the base fabric slightly warped which results in the deformation of the spiral arms. The changes in the spiral dimensions degraded the circular polarisation. Meanwhile, the effects of the positioner and the supporting structure for the phantom in the anechoic chamber can also affect the near-field scanning results.

6 Conclusions

This paper has reported a spiral antenna that can utilise the available area of the human torso for off-body wide-band communications. The antenna has been simulated assuming the conductivity and thickness of the conducting thread. The broad-band performance of the spiral antenna were measured and compared with simulated results showing the viability of the antenna for on-body use. The efficiency of the antenna was very sensitive to the distance away from the phantom with larger distances resulting in higher efficiencies. Simulated efficiencies of up to 75% were obtained with 17 mm separations. The efficiency increased with frequency due to the larger antenna–phantom separation and also the reduced skin depth effects of the conducting thread. The effect of curving the antenna around the torso compared with the planar antenna was minimal. The stability of the simulated S_{11} and AR with different curvatures and spacings indicated that the antenna would function on different users.

The fabrication of the embroidered spiral was a challenging process. The tension of the threads caused warping of the substrate and also the antenna. The embroidered spiral showed reasonable agreement with the simulations in terms of the S_{11}. A novel near-field scanning system has been utilised and the data was transformed to the far field. The far-field radiation efficiency that computed from near-field measurements of the embroidered spiral antenna on the SAM phantom varied between 10 and 25% from 1.6 to 2.6 GHz when in the worst-case scenario of being placed flush against the torso. These results are reasonable considering the proximity of the antenna to the torso and the finite conductivity of the embroidered thread. The measured AR was slightly larger than in the simulations as is often the case with embroidered antennas due to the complex stitch pattern.

7 References

1 Post, E.R., Orth, M., Russo, P.R., *et al.*: 'E-broidery: design and fabrication of textile-based computing', *IBM Syst. J.*, 2000, **39**, (3.4), pp. 840–860
2 Matthews, J.C.G., Pettitt, G.: 'Development of flexible, wearable antennas'. European Conf. on Antennas & Propagation (EuCAP), 2009, pp. 273–277
3 Hall, P.S., Hao, Y.: 'Antennas and propagation for body-centric wireless communications' (Artech House, Boston, USA, 2012)
4 Abufanas, H., Hadi, R.J., Sandhagen, C., *et al.*: 'New approach for design and verification of a wideband Archimedean spiral antenna for radiometric measurement in biomedical applications'. 2015 German Microwave Conf., 2015, pp. 127–130
5 Kiourti, A., Lee, C., Volakis, J.L.: 'Fabrication of textile antennas and circuits with 0.1 mm precision', *IEEE Antennas Wirel. Propag. Lett.*, 2016, **15**, pp. 151–153
6 Ivsic, B., Galoic, A., Bonefacic, D.: 'Embroidered textile logarithmic spiral antenna and its energy efficiency'. 2015 57th Int. Symp. ELMAR (ELMAR), 2015, pp. 157–160
7 Tsolis, A., Whittow, W.G., Alexandridis, A.A., *et al.*: 'Embroidery and related manufacturing techniques for wearable antennas: challenges and opportunities', *Electronics*, 2014, **3**, (2), pp. 314–338
8 Zhang, L., Wang, Z., Psychoudakis, D., *et al.*: 'E-fiber electronics for body-worn devices'. 2012 Sixth European Conf. on Antennas and Propagation (EUCAP), 2012, pp. 760–761
9 Roh, J.-S., Chi, Y.-S., Lee, J.-H., *et al.*: 'Embroidered wearable multiresonant folded dipole antenna for FM reception', *IEEE Antennas Wirel. Propag. Lett.*, 2010, **9**, pp. 803–806
10 Seager, R.D., Zhang, S., Chauraya, A., *et al.*: 'Effect of the fabrication parameters on the performance of embroidered antennas', *IET Microw. Antennas Propag.*, 2013, **7**, (14), pp. 1174–1181
11 Cottet, D., Grzyb, J., Kirstein, T., *et al.*: 'Electrical characterization of textile transmission lines', *IEEE Trans. Adv. Packag.*, 2003, **26**, (2), pp. 182–190
12 Karlsson, K., Carlsson, J.: 'Wideband characterization of fabrics for textile antennas'. Sixth European Conf. on Antennas and Propagation (EuCAP), 2012, pp. 1358–1361
13 Lee, H., Tentzeris, M.M., Geiger, J.: 'Flexible spiral antenna with microstrip tapered infinite balun for wearable applications'. Proc. 2012 IEEE Int. Symp. on Antennas and Propagation, 2012, pp. 1–2
14 Zhong, J., Kiourti, A., Sebastian, T., *et al.*: 'Conformal load-bearing spiral antenna on conductive textile threads', *IEEE Antennas Wirel. Propag. Lett.*, 2016, pp. 1–1
15 Wang, Z., Lee, L.Z., Volakis, J.L.: 'A 10:1 bandwidth textile-based conformal spiral antenna with integrated planar balun'. IEEE Antennas and Propagation Society, AP-S Int. Symp. (Digest), 2013, pp. 220–221
16 Zhang, S., Speight, D., Paraskevopoulos, A., *et al.*: 'On-body measurements of embroidered spiral antenna'. Loughborough Antennas & Propagation Conf. (LAPC), 2015
17 'MCL-T whole-body solid SAM phantom'. Available at http://www.mcluk.org/solidbodies.php, accessed 22 December 2015
18 International Commission on Non-Ionizing Radiation Protection (ICNIRP): 'Health issues related to the use of handheld radio telephones and base transmitters', *Health Phys.*, 1996, **70**, (4), pp. 383–387
19 'Liberator Fiber'. Available at http://www.metalcladfibers.com/liberator-fiber/, accessed 10 June 2015
20 Parini, C., Gregson, S., McCormick, J., *et al.*: 'Theory and practice of modern antenna range measurements' (The IET, London, UK, 2014)